Journal of Composites and Compounds 5 (2023) 179-189

Available online at www.jourcc.com

Journal homepage: www.JOURCC.com

Journal of Composites and Compounds

A short review on the photocatalytic degradation of ofloxacin in aqueous media

Alomari Asma Dhahawi Ahmad [a], *Alamri Rahmah Dhahawi Ahmad* [b, *]

[a] *Chemistry Department, Al-Qunfudah University College, Umm Al-Qura University, Al-Qunfudah 1109, Saudi Arabia*
[b] *Al Mukhwah Education Directorate, Ministry of Education 65441, Saudi Arabia*

A B S T R A C T

Among the commonly used advanced oxidation processes (AOPs) commonly employed in wastewater remediation, photocatalytic remediation has remained prominent and promising. This is because the process is effective in degrading and even mineralizing numerous organic pollutants including ofloxacin. In view of that, various categories photocatalysts such as titanium-based, zinc-based, bismuth-based, silver-based, and others have been and are still continuously tested by various researchers in remediating wastewater contaminated by pollutants such as ofloxacin. This short review focuses on reviewing some publications, especially those reported in the last decade involving photocatalytic degradation of ofloxacin in aqueous media.

A R T I C L E I N F O R M A T I O N

Article history:
Received 14 May 2023
Received in revised form 26 June 2023
Accepted 28 August 2023

Keywords:
Ofloxacin
Photocatalytic degradation
Photocatalysts
UV-light
Visible light

Table of contents

1. Introduction

Water pollution has remained one of the leading global environmental challenges, following the discharge of toxic substances from various anthropogenic activities [1]. Among the toxic substances being discharged, a group of contaminants, including pharmaceuticals and personal care products (PPCPs), contrast media, plasticizers, nanomaterials, flame retardants, surfactants, food additives, wood preservatives, pesticides, hormones etc., have been recognized as significant water pollutants and are termed as *emerging contaminants* (ECs).

As a class of ECs, PPCPs are also components with a high concentration in wastewater, amongst which antibiotics have received significant attention due to their impact on the microbial community [2, 3]. Among the antibiotics, fluoroquinolones, including ofloxacin (OFL), are frequently detected in wastewaters and surface waters [4, 5]. It is also reported that the techniques currently employed by most wastewater treatment plants (WWTPs) have limited capacity for the thorough elimination of PPCPs, including OFL from wastewater [6].

Ofloxacin (Table 1) is a second-generation fluoroquinolone antibiotic with the chemical formula of $C_{18}H_{20}FN_3O_4$ and chemical name 9-fluoro-2,3-dihydro-3-methyl-10-(4-methyl-1-piperazynyl)-7-oxo-7H-pyrido-[1,2,3-de]-1,4-benzoxazine-6-carboxylic acid [7, 8]. It was patented in 1980 and subsequently approved for medical use in 1985 [9, 10]. Currently, OFL is frequently prescribed for the treatment of bronchitis, infectious diarrhoea, pneumonia, chlamydia, pelvic inflammatory disease, eye infections, digestive infections, ear infections, gonorrhoea, respiratory tract infections, urinary tract infections, gastrointestinal infections, and skin infections [11-13].

* *Corresponding author: Alamri Rahmah Dhahawi Ahmad; E-mail: t337472@bg.moe.gov.sa*

https://doi.org/10.61186/jcc.5.3.3

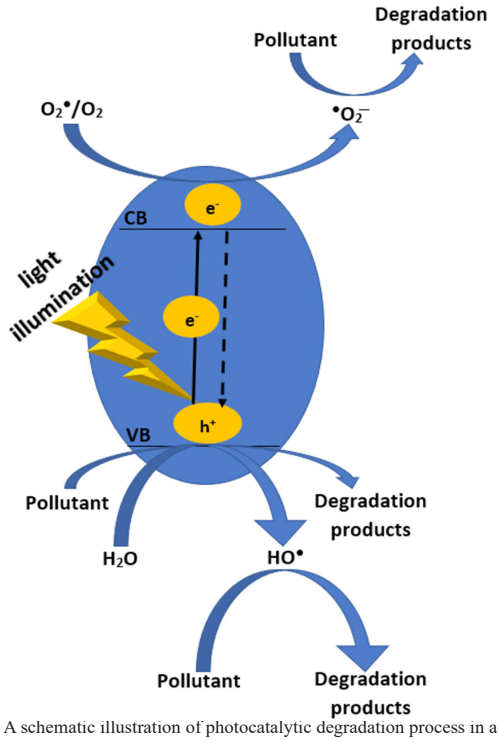

Fig. 1. A schematic illustration of photocatalytic degradation process in a semiconductor material.

However, due to its partial metabolism in the body after ingestion, biological resistance, and the large volume of pharmaceutical wastewater which is being released untreated, studies have reported the detection of OFL with different concentrations in hospital wastewater (25,000 – 35,000 ng/L), municipal wastewater treatment plants (53 – 1800 ng/L) and surface water (10 – 535 ng/L), with a residence time of about 10.6 days [14-16].

Nowadays, the well-known methods commonly employed to remove persistent organic contaminants, including OFL, are the Advanced Oxidation Processes (AOPs) of which photocatalytic degradation is prominent. These processes involve generating highly reactive and non-selective free radical species, which can destroy many organic pollutants. The AOPs are currently categorized as environmentally friendly processes since they neither result in secondary pollution nor the generation of excessive hazardous sludge [17-19]. In this regard, the present work reviewed variety of photocatalysts used by various researchers in treating wastewater contaminated by OFL.

2. Exposure effects of OFL on environment and living organisms.

Residual OFL pose a serious threat to both the ecological environment and the human health [20]. For instance, the presence of OFL in water results in high colour with unpleasant odours [10, 21]. It can results in acute toxicity (when presents in mg/L) and chronic toxicity (when presents in µg/L) to aquatic organisms [22]. The presence of OFL may also lead to microbial resistance among pathogens/generation of superbugs or the death of microorganisms effective in wastewater remediation [14, 21, 23]. For humans, low concentrations of OFL could be enriched into the human body through the food chain [23]. The development of antibiotic resistant bacteria could be a potential harm for people's ability to defeat those bacterial strains [24, 25]. After long-term exposure, OFL may also pose considerable health risk leading to dizziness, abdominal pain and numbness of limbs [26]. Thus, identifying the proper processes for the thorough and complete elimination of OFL from wastewater is essential.

3. Mechanism of photocatalytic degradation

The degradation of pollutants via semiconductor photocatalysis is initiated through illumination of the material (e.g TiO_2, ZnO, BiOBr etc.) with light of sufficient wavelength. This leads to the migration of electrons from valence band (VB) to conduction band (CB), producing electron-hole pairs. However, if the challenge of charge pairs recombination is successfully overcomed, the holes (h^+) at the valence band (VB), depending on their oxidizing power could degrade the pollutants directly or oxidizes water (H_2O) to generate hydroxyl radicals ($HO^{\bullet}$) for subsequent degradation of the pollutant. The electrons at the conduction band (CB) convert oxygen (O_2) to superoxide radical anions ($^{\bullet}O_2^-$), which also degrade pollutants. The schematic illustration of the process is shown in Figure 1. However, it should be mentioned that the degradation pathway of organic pollutants including OFL is very subjective, and the pathway varies greatly from study to study.

Figure 1: A schematic illustration of photocatalytic degradation process in a semiconductor material.

4. Performance assessment of photocatalysts in OFL degradation

Over the years, various researchers have made consistent efforts to eradicate pollutants including OFL from wastewater via photocatalytic degradation process. Among the materials reported in the process are the TiO_2-based photocatalysts, ZnO-based photocatalysts, Bi-based photocatalysts are prominent. Although the photocatalysts are sometimes being augmented using strategies such as doping and formation of het-

Table 1.
Molecular structure and some physicochemical properties of OFL

Property		Reference
Chemical formula	$C_{18}H_{20}FN_3O_4$	[54]
CAS number	82419-36-1	[55]
Therapeutic group	Antibiotic	[56]
Chemical structure	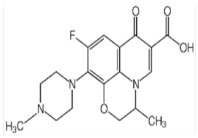	[57]
Molecular weight (g/mol)	361.4	[58]
Color	White	[59]
Melting point	270 – 273 ºC	[56]
Solubility in water at 25 ºC (mg/mL)	60 (pH = 2 – 5); 4 (pH = 7); 303 (pH = 9.8)	[60]
Partition coefficient	-0.39	[55]
Dissociation constant	6.10/8.28	[55]
Octanol/water partition coefficient log $k_{o/w}$	0.41 (pH 7); 0.33 (pH 7.2); 0.28 (pH 7.3)	[56]
Isoelectric constants	pKa_1 = 5.97; pKa_2 = 9.28	[61]
Vapour pressure (mm Hg)	1.55E-0.13	[56]
Henry constant at 25 ºC (atm m^{-3} $mole^{-1}$)	4.98E-0.20	[56]
Pharmacokinetic parameters	Bioavailability (%) = 70-90 Time of half-life (h) = 5-7.4 Excretion in urine (%) = 80	[56]

Table 2.
List of various photocatalysts and their efficiencies in degrading OFL.

S/N	Catalyst	Dosage (g/L)	C_{OFL} (mg/L)/ V_{OFL} (mL)	pH	Light source	Kinetics model	Rate constant	Time (min)	Efficiency (%)	Reference
					Titanium-based photocatalysts					
1	TiO_2	0.5	25/-	7	Solar radiation (70.3 Klux)	-	-	120	32.5	[41]
2	Degussa TiO_2	1.5	25/-	3	UV 36 W (365 nm)	Pseudo 1st order	0.0036 min^{-1}	360	72	[33]
3	Degussa TiO_2	1.5	25/-	4	UV 36 W (365 nm)	-	-	360	~62	[33]
4	Degussa TiO_2	1.5	25/-	5	UV 36 W (365 nm)	-	-	360	~65	[33]
5	Degussa TiO_2	1.5	25/-	6	UV 36 W (365 nm)	-	-	360	~58	[33]
6	Degussa TiO_2	1.5	25/-	7	UV 36 W (365 nm)	-	-	360	~55	[33]
7	Degussa TiO_2	1.5	25/-	8	UV 36 W (365 nm)	-	-	360	~45	[33]
8	Degussa TiO_2	1.5	25/-	9	UV 36 W (365 nm)	-	-	360	~39	[33]
9	Degussa TiO_2	1.5	25/-	10	UV 36 W (365 nm)	-	-	360	~37	[33]
10	Degussa TiO_2	0.5	25/-	6	UV 36 W (365 nm)	-	-	360	~50	[33]
11	Degussa TiO_2	1	25/-	6	UV 36 W (365 nm)	-	-	360	~56	[33]
12	Degussa TiO_2	1.5	25/-	6	UV 36 W (365 nm)	-	-	360	72	[33]
13	Degussa TiO_2	2	25/-	6	UV 36 W (365 nm)	-	-	360	~58	[33]
14	Bi-Ni co-doped TiO_2	1.5	25/-	3	UV 36 W (365 nm)	-	-	360	86	[33]
15	Titanium dioxide nanoarray	-	25/-	4.8	Simulated sunlight	Pseudo 1st order	2.45 x 10^{-3} min^{-1}	120	25.5	[62]
16	TiO_2	0.4	*4x10^{-5}/100	-	150 W tungsten lamp	Pseudo 1st order	0.0017 min^{-1}	120	21.3	[34]
17	TiO_2-rGO	0.4	*4x10^{-5}/100	-	150 W tungsten lamp	Pseudo 1st order	0.0024 min^{-1}	120	28.3	[34]
18	TiO_2/CdS	4.5	10/100	-	85 W Oreva bulb with 4150 lumens intensity	-	-	180	86	[35]
19	B-TiO_2	0.4	40/50	-	20 W UV lamp (2300 $\mu W/cm^2$)	Pseudo 1st order	0.0248 min^{-1}	180	-	[63]
20	B-TiO_2(50%)/ iM16K	0.4	40/50	-	20 W UV lamp (2300 $\mu W/cm^2$)	Pseudo 1st order	0.0233 min^{-1}	180	-	[63]
21	TiO_2	0.45	10/100	7	85 W Oreva CFL bulb	Pseudo 1st order	0.00406 min^{-1}	180	65	[32]
22	Cu-doped TiO_2	0.45	10/100	7	85 W Oreva CFL bulb	Pseudo 1st order	0.00447 min^{-1}	180	72	[32]
23	P25	0.05	10/100	-	Simulated sunlight	Pseudo 2nd order	2.21 L $mmol^{-1}$ min^{-1}	180	91.4	[64]
24	TiO_2 (300 ºC)	0.04	20/250	-	100 W LED light with output of 40k Lux	-	-	180	90	[65]
25	TiO_2 (400 ºC)	0.04	20/250	-	100 W LED light with output of 40k Lux	-	-	180	76	[65]
					Zinc-based photocatalysts					
1	ZnO	0.25	10/200	-	15 W Panasonic cool daylight lamp	Pseudo 1st order	0.0017 min^{-1}	120	22	[66]
2	ZnO-Bi_2MoO_6	0.25	10/200	-	15 W Panasonic cool daylight lamp	Pseudo 1st order	0.0179 min^{-1}	120	94	[66]
3	ZnO	2	10/50	-	Xenon lamp (400 W, λ > 420 nm)	Pseudo 1st order	0.0029 min^{-1}	90	20	[67]
4	ZnO/MoS_2	2	10/50	-	Xenon lamp (400 W, λ > 420 nm)	Pseudo 1st order	0.0062 min^{-1}	90	52	[67]
5	ZnO	0.25	10/100	7	65 – 70 Klux	Pseudo 1st order	0.0108 min^{-1}	150	82	[38]
6	Silver modified ZnO	0.25	10/100	7	65 – 70 Klux	Pseudo 1st order	0.0266 min^{-1}	150	98	[38]
7	ZnO	0.2	**32/50	-	Halogen lamp	Pseudo 1st order	0.0031 min^{-1}	150	-	[68]
8	ZnO/2Cs_xWO_3	0.2	**32/50	-	Halogen lamp	Pseudo 1st order	0.00624 min^{-1}	150	-	[68]
9	ZnO	0.25	10/200	-	UV light	Pseudo 1st order	0.0119 min^{-1}	120	-	[69]
10	ZnO/CdS	0.25	10/200	-	UV light	Pseudo 1st order	0.0106 min^{-1}	120	-	[69]
11	ZnO	0.25	10/200	-	Visible light	Pseudo 1st order	0.0021 min^{-1}	120	-	[69]
12	ZnO/CdS	0.25	10/200	-	Visible light	Pseudo 1st order	0.0086 min^{-1}	120	-	[69]
13	ZnO	0.25	10/200	-	Mercury lamp (125 W)	Pseudo 1st order	0.0037 min^{-1}	180	-	[39]
14	Ag-ZnO	0.25	10/200	-	Mercury lamp (125 W)	Pseudo 1st order	0.0132 min^{-1}	180	-	[39]

Table 2.
(Continued)

S/N	Catalyst	Dosage (g/L)	C_{OFL} (mg/L)/ V_{OFL} (mL)	pH	Light source	Kinetics model	Rate constant	Time (min)	Efficiency (%)	Reference
					Silver-based photocatalysts					
1	$AgFeO_2$	0.4	10/50	-	5 W white LED 73 $mW.cm^{-2}$ (PCX 50 B)	Pseudo 2nd order	0.00735 $L.mg^{-1}.min^{-1}$	60	22.5	[70]
2	$AgFeO_2$-Bi_4TaO_8Cl	0.4	10/50	-	5 W white LED 73 $mW.cm^{-2}$ (PCX 50 B)	Pseudo 2nd order	0.10638 $L.mg^{-1}.min^{-1}$	60	37.5	[70]
3	Ag_3PO_4	0.5	10/500	-	500 W xenon lamp	-	-	30	70.3	[71]
4	Ag_3PO_4/g-C_3N_4	0.5	10/500	-	500 W xenon lamp	-	-	10	71.9	[71]
5	AgBr	0.25	10/200	-	Visible irradiation	Pseudo 1st order	0.0134 min^{-1}	-	-	[40]
6	AgBr/WO_3	0.25	10/200	-	Visible irradiation	Pseudo 1st order	0.0057 min^{-1}	240	68	[40]
7	AgBr	0.25	10/200	-	UV irradiation	Pseudo 1st order	0.0088 min^{-1}	-	-	[40]
8	AgBr/WO_3	0.25	10/200	-	UV irradiation	Pseudo 1st order	0.0046 min^{-1}	240	55	[40]
9	AgBr	0.25	10/200	-	Solar light irradiation	Pseudo 1st order	0.0279 min^{-1}	-	-	[40]
10	AgBr/WO_3	0.25	10/200	-	Solar light irradiation	Pseudo 1st order	0.0436 min^{-1}	240	85	[40]
11	Ag_2O-C_3N_4	0.5	10/100	6	Xe lamp (PLS-SXE300)	-	-	5	99.1	[72]
					Bismuth-based photocatalysts					
1	Bi_4TaO_8Cl	0.4	10/50	-	5 W white LED 73 $mW.cm^{-2}$ (PCX 50 B)	Pseudo 2nd order	0.00721 $L.mg^{-1}.min^{-1}$	60	29.7	[70]
2	Bi_2MoO_6	1	10/100	-	Sunlight (55 – 65 Lux)	-	-	90	71	[73]
	Bi_2MoO_6	0.25	10/200	-	15 W Panasonic cool daylight lamp	Pseudo 1st order	0.0092 min^{-1}	120	82	[66]
3	Bi_2S_3	1	-	-	150 W Xe lamp (100 mW/cm^2)	Pseudo 1st order	1.3 x 10^{-3} min^{-1}	180	21	[74]
4	Bi_2WO_6	1	-	-	150 W Xe lamp (100 mW/cm^2)	Pseudo 1st order	8.2 x 10^{-3} min^{-1}	180	78	[74]
5	Bi_2S_3/Bi_2WO_6	1	-	-	150 W Xe lamp (100 mW/cm^2)	Pseudo 1st order	11.2 x 10^{-3} min^{-1}	180	87	[74]
6	Bi_2O_3	0.5	25/-	7	Solar radiation (70.3 Klux)	-	-	120	75	[41]
7	Bi_2O_3/TiO_2	0.5	25/-	7	Solar radiation (70.3 Klux)	-	-	120	92.4	[41]
7	Bi_2WO_6	0.4	10/50	-	50 W energy-saving LED lamp	Pseudo 1st order	0.0347 min^{-1}	30	~70	[42]
8	Bi_2WO_6/Fe_3O_4	0.4	10/50	-	50 W energy-saving LED lamp	Pseudo 1st order	0.1295 min^{-1}	30	~99	[42]
9	Bi_2WO_6/Fe_3O_4/BC	0.4	10/50	-	50 W energy-saving LED lamp	Pseudo 1st order	0.1835 min^{-1}	30	~100	[42]
10	$BiFeO_3$	0.5	10/100	8	CFL Bulb (85W, 4150 lumens, oreva)	Pseudo 1st order	0.0097 min^{-1}	180	80	[44]
11	Bi_3O_4Cl	0.5	5/100	-	300 W Xe lamp (λ > 400 nm)	Pseudo 1st order	0.0144 min^{-1}	80	66.8	[75]
12	Bi_3O_4Cl/$LaVO_4$	0.5	5/100	-	300 W Xe lamp (λ > 400 nm)	Pseudo 1st order	0.0344 min^{-1}	80	94.3	[75]
12	Bi_2MoO_6	0.4	5/50	-	300 W xenon lamp	Pseudo 1st order	0.02978 min^{-1}	40	46	[45]
13	Cd- Bi_2MoO_6	0.4	5/50	-	300 W xenon lamp	Pseudo 1st order	0.04839 min^{-1}	40	~90	[45]
14	Bi_2MoO_6	0.4	*4x10^{-5}/100	-	150 W tungsten lamp	Pseudo 1st order	0.0041 min^{-1}	120	~38	[34]
15	Bi_2MoO_6-rGO	0.4	*4x10^{-5}/100	-	150 W tungsten lamp	Pseudo 1st order	0.0055 min^{-1}	120	41.2	[34]
16	Bi_2MoO_6-TiO_2	0.4	*4x10^{-5}/100	-	150 W tungsten lamp	Pseudo 1st order	0.0090 min^{-1}	120	67.2	[34]
17	Bi_2MoO_6-rGO-TiO_2	0.4	*4x10^{-5}/100	-	150 W tungsten lamp	Pseudo 1st order	0.0174 min^{-1}	120	92.3	[34]
18	BiOCl	0.1	5/50	-	300 W xenon lamp	Pseudo 1st order	0.0021 min^{-1}	60	~20	[76]
19	BiOCl/$NaNbO_3$	0.1	5/50	-	300 W xenon lamp	Pseudo 1st order	0.016 min^{-1}	60	90	[76]
20	Bi_2MoO_6	1	10/30	-	150 W xenon lamp	Pseudo 1st order	0.0023 min^{-1}	100	40	[77]
21	Bi_4TaO_8Cl-bulk	0.4	20/50	-	5 W white LED (72.9 $mW.cm^{-2}$)	Pseudo 1st order	0.00250 min^{-1}	150	34.9	[78]

Table 2.
(Continued)

S/N	Catalyst	Dosage (g/L)	C_{OFL} (mg/L)/ V_{OFL} (mL)	pH	Light source	Kinetics model	Rate constant	Time (min)	Efficiency (%)	Reference
22	Bi_4TaO_8Cl	0.4	20/50	-	5 W white LED (72.9 mW.cm^{-2})	Pseudo 1st order	0.01454 min^{-1}	150	84.2	[78]
23	Bi_2O_3	0.3	10/100	5	350 W xenon lamp	Pseudo 1st order	0.01152 min^{-1}	90	68.6	[79]
24	Bi_2O_7I	0.1	10/100	-	500 W xenon lamp	Pseudo 1st order	0.0046 min^{-1}	180	55.1	[43]
25	Bi_2O_7I/ MWCNTs	0.1	10/100	-	500 W xenon lamp	Pseudo 1st order	0.0129 min^{-1}	180	88.2	[43]
					Others					
1	$CeTi_2O_6$	0.4	20/50	-	20 W lamp (2300 µW/cm^2)	Pseudo 1st order	6.852 x 10^{-2} min^{-1}	50	67.9	[80]
2	$Gd_2Ti_2O_7$	0.4	20/50	-	20 W UV lamp (2300 µW/cm^2)	Pseudo 1st order	7.8 x 10^{-3} min^{-1}	90	50.4	[81]
3	$Gd_2Ti_2O_7/SiO_2$	0.4	20/50	-	20 W UV lamp (2300 µW/cm^2)	Pseudo 1st order	1.7 x 10^{-2} min^{-1}	90	79.1	[81]
4	g-C_3N_4	0.1	15/100	-	Microsolar 300A (100 mW/cm^2)	Pseudo 1st order	0.0168 min^{-1}	30	21.1	[82]
5	$NaNbO_3$	0.1	15/100	-	Microsolar 300A (100 mW/cm^2)	Pseudo 1st order	0.0059 min^{-1}	30	42.5	[82]
6	g-C_3N_4/ $NaNbO_3$	0.1	15/100	-	Microsolar 300A (100 mW/cm^2)	Pseudo 1st order	0.1745 min^{-1}	30	99.5	[82]
7	CdS	0.25	10/100	9	85 W Oreva CFL bulb, 4150 lumens, λ = 450–650 nm	Langmuir-Hinshelwood model	0.02217 min^{-1}	80	79.5	[83]
8	UiO-66/wood	0.02	10/35	6	Simulated sunlight	Pseudo 1st order	40.5 x 10^{-4}min^{-1}	270	-	[53]
9	UiO-66	0.02	10/35	6	Simulated sunlight	Pseudo 1st order	33.2 x 10^{-4}min^{-1}	270	-	[53]
10	Wood	0.02	10/35	6	Simulated sunlight	Pseudo 1st order	27.2 x 10^{-4}min^{-1}	270	-	[53]
11	g-C_3N_4	0.5	10/500	-	500 W xenon lamp	-	-	30	4.9	[71]
12	$Sm_2Ti_2O_7$	-	20/50	-	20 W UV light	Pseudo 1st order	0.00977 min^{-1}	70	53.9	[50]
13	$Sm_2Ti_2O_7$ supported on quartz sand	-	20/50	-	20 W UV light	Pseudo 1st order	0.0220 min^{-1}	70	78.6	[50]
14	CQDs@CoO/ La_2O_3/NiO TONCs	0.2	20/100	-	-	Pseudo 1st order	0.036 min^{-1}	60	91.24	[84]
15	CoO/La_2O_3/ NiO TONPs	0.2	20/100	-	-	Pseudo 1st order	0.018 min^{-1}	60	69.70	[84]
16	La_2O_3	0.2	20/100	-	-	Pseudo 1st order	0.007 min^{-1}	60	34.63	[84]
17	NiO	0.2	20/100	-	-	Pseudo 1st order	0.005 min^{-1}	60	27.72	[84]
18	CoO	0.2	20/100	-	-	Pseudo 1st order	0.003 min^{-1}	60	17.45	[84]
19	$Sm_2Ti_2O_7$	0.6	20/50	-	20 W UV lamp	Pseudo 1st order	0.00402 min^{-1}	150	45.1	[51]
20	$Sm_2Ti_2O_7$/ NaZSM-5	0.6	20/50	-	20 W UV lamp	Pseudo 1st order	0.00769 min^{-1}	150	70.0	[51]
21	$Sm_2Ti_2O_7$/ 0.3HZSM-5	0.6	20/50	-	20 W UV lamp	Pseudo 1st order	0.0163 min^{-1}	150	93.5	[51]
22	CdS	2	10/50	-	Xenon lamp (400 W, λ > 420 nm)	Pseudo 1st order	0.0036 min^{-1}	90	27.5	[67]
23	MoS_2	2	10/50	-	Xenon lamp (400 W, λ > 420 nm)	Pseudo 1st order	0.0031 min^{-1}	90	25.1	[67]
24	CdS/MoS_2	2	10/50	-	Xenon lamp (400 W, λ > 420 nm)	Pseudo 1st order	0.0075 min^{-1}	90	61	[67]
25	CdS/MoS_2/ ZnO	2	10/50	-	Xenon lamp (400 W, λ > 420 nm)	Pseudo 1st order	0.024 min^{-1}	90	89	[67]
26	g-C_3N_4	0.5	10/100	7	150 W/cm^2 tungsten lamp	-	-	70	48.6	[85]
27	$MnWO_4$	0.5	10/100	7	150 W/cm^2 tungsten lamp	-	-	70	39.1	[85]

Table 2.
(Continued)

S/N	Catalyst	Dosage (g/L)	C_{OFL} (mg/L)/ V_{OFL} (mL)	pH	Light source	Kinetics model	Rate constant	Time (min)	Efficiency (%)	Reference
28	$MnWO_4$@ g-C_3N_4	0.5	10/100	7	150 W/cm^2 tungsten lamp	-	-	70	90.4	[85]
29	$LaVO_4$	0.5	5/100	-	300 W Xe lamp (λ > 400 nm)	Pseudo 1st order	0.0003 min^{-1}	80	2.5	[75]
30	Co-MIL-53-NH_2-BT	0.25	10/20	-	500 W Xe lamp (λ > 400 nm)	Pseudo 1st order	0.0392 min^{-1}	120	99.8	[86]
31	Mn_2O_3/SiO_2	0.7	10/20	-	45 W Philips lamp (100 W/m^2)	Pseudo 1st order	0.0096 min^{-1}	120	73.2	[87]
32	In_2S_3	-	25/-	4.8	Simulated sunlight	Pseudo 1st order	2.59 x 10^{-3} min^{-1}	120	26.8	[62]
33	In_2S_3/titanium dioxide nanoarray	-	25/-	4.8	Simulated sunlight	Pseudo 1st order	5.24 x 10^{-3} min^{-1}	120	92.7	[62]
34	Cs_xWO_3	0.2	**32/50	-	Halogen lamp	Pseudo 1st order	0.00293 min^{-1}	150	-	[68]
35	NiCr-LDH	0.5	15/50	-	High-pressure mercury lamp (300 W)	Pseudo 1st order	0.0063 min^{-1}	150	-	[88]
36	NiCr-LDH/ PSB	0.5	15/50	-	High-pressure mercury lamp (300 W)	Pseudo 1st order	0.0218 min^{-1}	150	-	[88]
37	ZnS/MoS_2/ Bi_2WO_6	0.4	10/50	5	500 W xenon lamp	Pseudo 1st order	0.01028 min^{-1}	120	83.7	[89]
38	$La_2Ti_2O_7$	0.6	40/50	-	2300 μW/cm^2 (wavelength 253.7 nm)	Pseudo 1st order	0.025 min^{-1}	120	95.0	[46]
39	$Gd_2Ti_2O_7$	0.4	20/50	6.5	20 W UV lamp (2300 μW/cm^2)	Pseudo 1st order	1.05 x 10^{-2} min^{-1}	30	27.5	[90]
40	$Gd_2Ti_2O_7$/ HZSM-5	0.4	20/50	6.5	20 W UV lamp (2300 μW/cm^2)	Pseudo 1st order	3.52 x 10^{-2} min^{-1}	30	54.5	[90]
41	WO_3	0.25	10/200	-	Visible irradiation	Pseudo 1st order	0.0004 min^{-1}	-	-	[40]
42	WO_3	0.25	10/200	-	UV irradiation	Pseudo 1st order	0.0022 min^{-1}	-	-	[40]
43	WO_3	0.25	10/200	-	Solar light irradiation	Pseudo 1st order	0.0059 min^{-1}	-	-	[40]
44	$NaNbO_3$	0.1	5/50	-	300 W xenon lamp	Pseudo 1st order	0.002 min^{-1}	60	~20	[76]
45	MoO_3	1	20/-	-	150 W xenon lamp	Pseudo 1st order	-	100	41	[91]
46	C_3N_4	1	20/-	-	150 W xenon lamp	Pseudo 1st order	-	100	39	[91]
47	Ag/C_3N_4	1	20/-	-	150 W xenon lamp	Pseudo 1st order	5.3 x 10^{-3} min^{-1}	100	47	[91]
48	MoO_3/C_3N_4	1	20/-	-	150 W xenon lamp	Pseudo 1st order	8.46 x 10^{-3} min^{-1}	100	54	[91]
49	MoO_3/Ag/C_3N_4	1	20/-	-	150 W xenon lamp	Pseudo 1st order	17.84 x 10^{-3} min^{-1}	100	96	[91]
50	CdS	0.25	10/200	-	UV light	Pseudo 1st order	0.0096 min^{-1}	120	-	[69]
51	CdS	0.25	10/200	-	Visible light	Pseudo 1st order	0.0070 min^{-1}	120	-	[69]
52	C_3N_4	0.5	10/100	6	Xe lamp (PLS-SXE300)	-	-	15	14.6	[72]
53	MoS_2	1	10/30	-	150 W xenon lamp	Pseudo 1st order	0.0033 min^{-1}	100	32	[77]
54	MoS_2/Bi_2MoO_6	1	10/30	-	150 W xenon lamp	Pseudo 1st order	0.0180 min^{-1}	100	98.4	[77]
55	$CeTi_2O_6$ (600 °C)	0.4	20/50	-	20 W lamp (2300 μW/cm^2)	-	-	30	31.2	[52]
56	$CeTi_2O_6$ (800 °C)	0.4	20/50	-	20 W lamp (2300 μW/cm^2)	-	-	30	56.7	[52]
57	ZnCdS	-	30/-	-	300 W xenon lamp (λ ≥ 420 nm)	Pseudo 1st order	0.0130 min^{-1}	90	75.8	[49]
58	$ZnIn_2S_4$	-	30/-	-	300 W xenon lamp (λ ≥ 420 nm)	Pseudo 1st order	0.0138 min^{-1}	90	78.6	[49]
59	g-C_3N_4	-	30/-	-	300 W xenon lamp (λ ≥ 420 nm)	Pseudo 1st order	0.0049 min^{-1}	90	52.5	[49]
60	g-C_3N_4-vTA	-	30/-	-	300 W xenon lamp (λ ≥ 420 nm)	Pseudo 1st order	0.0098 min^{-1}	90	65.4	[49]

Table 2.
(Continued)

S/N	Catalyst	Dosage (g/L)	C_{OFL} (mg/L)/ V_{OFL} (mL)	pH	Light source	Kinetics model	Rate constant	Time (min)	Efficiency (%)	Reference
61	ZnCdS@ $ZnIn_2S_4$	-	30/-	-	300 W xenon lamp (λ ≥ 420 nm)	Pseudo 1st order	0.0161 min^{-1}	90	86.4	[49]
62	ZnCdS@ $ZnIn_2S_4$@g-C_3N_4-vTA	-	30/-	-	300 W xenon lamp (λ ≥ 420 nm)	Pseudo 1st order	0.0256 min^{-1}	90	95.7	[49]
63	Bulk g-C_3N_4	0.5	30/100	-	300 W xenon lamp (PLS-SXE 300/300 UV)	Pseudo 1st order	0.006 min^{-1}	-	-	[92]
64	P doped g-C_3N_4	0.5	30/100	-	300 W xenon lamp (PLS-SXE 300/300 UV)	Pseudo 1st order	0.009 min^{-1}	90	38.4	[92]
65	MIL-88A(Fe)	0.5	30/100	-	300 W xenon lamp (PLS-SXE 300/300 UV)	Pseudo 1st order	0.003 min^{-1}	90	50.6	[92]
66	P-CN100/MIL-88A	0.5	30/100	-	300 W xenon lamp (PLS-SXE 300/300 UV)	Pseudo 1st order	0.019 min^{-1}	90	95.6	[92]
67	$CoFe_2O_4$@ Bi_2O_3/NiO	0.3	10/100	5	350 W xenon lamp	Pseudo 1st order	0.03316 min^{-1}	90	95.2	[79]
68	NiO	0.3	10/100	5	350 W xenon lamp	Pseudo 1st order	0.00113 min^{-1}	90	50.5	[79]
69	g-C_3N_4	0.1	20/100	-	PLS-SXE300 Xe lamp	Pseudo 1st order	0.00214 min^{-1}	200	-	[93]
70	PCN-222	0.1	20/100	-	PLS-SXE300 Xe lamp	Pseudo 1st order	0.00361 min^{-1}	200	-	[93]
71	PCN-222/g-C_3N_4	0.1	20/100	-	PLS-SXE300 Xe lamp	Pseudo 1st order	0.01448 min^{-1}	200	95.9	[93]
72	CdS	0.05	10/100	-	Simulated sunlight	Pseudo 2nd order	2.21 L $mmol^{-1}$ min^{-1}	180	72.9	[64]
73	UiO-67/CdS	0.05	10/100	-	Simulated sunlight	Pseudo 2nd order	2.21 L $mmol^{-1}$ min^{-1}	180	86.7	[64]
74	rGO/CdS	0.05	10/100	-	Simulated sunlight	Pseudo 2nd order	2.21 L $mmol^{-1}$ min^{-1}	180	55.4	[64]
75	UiO-67/CdS/ rGO	0.05	10/100	-	Simulated sunlight	Pseudo 2nd order	2.21 L $mmol^{-1}$ min^{-1}	180	91	[64]
76	Fe_2O_3	0.05	10/100	-	Simulated sunlight	Pseudo 2nd order	2.21 L $mmol^{-1}$ min^{-1}	180	91.4	[64]
77	CdS	0.25	10/200	-	15 W daylight lamp	-	-	240	63	[47]
78	CdS	0.25	10/200	-	Sunlight	-	-	240	89	[47]
79	SWCNTs	0.1	20/50	-	300 W xenon lamp	Pseudo 1st order	0.008 min^{-1}	65	38.5	[48]
80	Hematite	0.1	20/50	-	300 W xenon lamp	Pseudo 1st order	0.014 min^{-1}	65	56.3	[48]
81	Fe_2O_3/ SWCNTs	0.1	20/50	-	300 W xenon lamp	Pseudo 1st order	0.019 min^{-1}	65	67.5	[48]
82	NH_2-MIL-125	0.1	20/50	-	300 W xenon lamp	Pseudo 1st order	0.032 min^{-1}	65	84.8	[48]
83	Fe_2O_3/CNTs/ MIL	0.1	20/50	-	300 W xenon lamp	Pseudo 1st order	0.065 min^{-1}	65	99.3	[48]

erojunctions for better results, notwithstanding, remarkable performances are still being recorded using pristine photocatalysts. Moreover, the interest in the process has led to the development of varieties of novel materials to serve as photocatalysts for the degradation of pollutants. Various categories photocatalysts including titanium-based, zinc-based, bismuth-based, silver-based and others have been used to degrade OFL and their efficiencies are summarized in Table 2.

4.1. Titanium-based photocatalysts

A prominent titanium-based photocatalyst frequently being used in the degradation of pollutants is titanium dioxide (TiO_2) [27]. It is cheap, non-toxic, and has strong oxidising power with long-term stability against chemical corrosion and photocorrosion [28, 29]. Despite these interesting features, TiO_2 has some limitations. For instance, it has a wide bandgap, which makes it active only upon irradiation with a UV light [27]. Similarly, the rate of chemical reaction with adsorbed species for redox reactions is slower compared to the rate of charge carriers recombination [30]. Fortunately, such challenges are often addressed via doping and formation of heterojunctions.

The impact of doping on the photocatalytic performance of TiO_2 towards degradation of OFL can be demonstrated using the works by Kaur et al. [31] and Bhatia et al. [32]. In the case of Kaur et al. [31], copper doped TiO_2 (Cu-doped TiO_2) was synthesized and used as photocatalyst to degrade OFL. Compared to pristine TiO_2 having a bandgap of 3.51 eV and specific surface area of 16.5 m^2/g, the bandgap and specific sur-

face area for Cu-doped TiO_2 were found to be 2.91 eV and 23.2 m^2/g, respectively. Within 180 min and at pH 7, 72% (rate constant of 0.00447 min^{-1}) of OFL (10 mg/L) was degraded over Cu-doped TiO_2 photocatalyst. Within similar time span, using 10 mg/L OFL at pH 7, 65% (rate constant of 0.00406 min^{-1}) degradation efficiency was recorded using pristine TiO_2.

The effect of Bi & Ni co-doping on TiO_2 towards photocatalytic degradation of OFL was studied by Bhatia et al. [32]. Under the conditions of pH 3, OFL concentration of 25 g/L, catalyst dosage of 1.5 g/L and using solar irradiation, 86% degradation efficiency was recorded in 6 h using Bi-Ni co-doped TiO_2, while performance using Degussa TiO_2 is 40%. However, the record under UV irradiation was 42.2% for Bi-Ni co-doped TiO_2 and 76% for Degussa TiO_2. Besides co-doping, Bhatia et al. [32], also studied the effect pH on the photocatalytic degradation of OFL using Degussa P25. Maximum degradation efficiency (72%) was recorded at pH 3. However, there was systematic decrease in efficiency as the pH rises from 5-10.

The use of TiO_2 based composites such as TiO_2-rGO and TiO_2/CdS as photocatalysts to degrade OFL have been reported by Raja et al. [33] and Kaur et al. [34]. The TiO_2-rGO had narrow band gap and lower photoluminescence intensity than pristine TiO_2, with photocatalytic degradation efficiency of 21.3 and 28.3% by TiO_2-rGO and TiO_2 towards OFL antibiotic. The lower band gap and separation of charge carriers contributed to the better performance by TiO_2-rGO. In the case of TiO_2/CdS composite, pristine TiO_2 had a band gap of 3.20 eV but decreased to 2.25 eV in the case of TiO_2/CdS. Similar pattern was observed in the case of photoluminescence. During degradation, 0.45 g/L of TiO_2 and TiO_2/CdS were able to degrade 65 and 86% of 10 mg/L OFL at pH 7. However, the performances recorded at pH 5 and 9 using TiO_2/CdS are 74.3 and 77.1%, respectively. Usually, the effect of pH on the degradation efficiency is attributed to the ionization state of the drug and catalyst and/or generated species (e.g. h^+, $^{\bullet}OH$) at low, neutral, or high pH active in the degradation of organic pollutants.

The role of calcination temperatures of 300, 350, 400 and 450 ºC on the features and performance of TiO_2 photocatalyst towards OFL degradation was studied by Mushtaq et al. [11]. The performance recorded using TiO_2 photocatalyst calcined at 300, 350, 400 and 450 ºC towards OFL degradation were 91, 87, 76 and 64%, respectively. The decrease in degradation efficiency with increase in calcination temperature is attributed to smaller surface area and larger particle size.

4.2. Zinc-based photocatalysts

A very famous zinc-based material used as photocatalyst is ZnO. It is an excellent II-IV semiconducting oxide with an exciton B.E of 60 meV and B.E of 3.37 eV [35]. Due to its high quantum efficiency and non-toxicity, ZnO is often considered as a replacement to TiO_2 [36]. Notwithstanding, ZnO exhibits low efficiency under solar irradiation with rapid recombination of charge carriers. However, both pristine and modified forms of ZnO have been using as photocatalysts to degrade OFL.

For instance, Kaur et al. [37] reported the use of pristine and silver modified ZnO as photocatalyst to degrade OFL in aqueous media. Compared to pristine ZnO which degraded 82% of 10 mg/L OFL within 150 min under solar irradiation, silver modified ZnO degraded 98%. The better performance recorded is due reduction in band gap from 3.23 eV in ZnO to 3.10 eV in silver modified ZnO, in addition to lower recombination rate of charge carriers in silver modified.

In a different study, Chankhanittha et al. [38] studied the effect of different light source on the activity of ZnO and Ag-ZnO towards degradation OFL. The degradation rate of ZnO towards OFL antibiotics was found to be 0.0037, 0.0020 and 0.0414 min^{-1} under UV, visible and natural sunlight. However, Ag-ZnO degraded OFL at the rate of 0.0132, 0.0036 and 0.0444 min^{-1} under UV, visible and natural sunlight. The better performance by Ag-ZnO is due to higher crystallinity, greater specific surface area, lower recombination of charge carriers and wider range of light response.

4.3. Silver-based photocatalysts

Various silver-based photocatalysts including $AgFeO_2$, Ag_3PO_4, AgBr and their composites have been reported to facilitate the degradation of OFL in aqueous media. For instance, Piriyanon et al. [39] reported the use of AgBr and AgBr/WO_3 as photocatalysts to degrade OFL. The degradation rates of AgBr towards OFL were found to be 0.0134, 0.0088 and 0.0279 min^{-1} under visible, UV and solar light irradiation. However, the performances using AgBr/WO_3 composite under visible, UV and solar light irradiation were 0.0057, 0.0046 and 0.0436 min^{-1}. Interestingly, under solar light irradiation, AgBr/WO_3 composite displayed much higher performance than AgBr, an effect mainly attributed to the suppression of electron-hole recombination and improved photo absorption. In generals, literatures reporting the degradation of OFL using silver-based photocatalysts are still lacking.

4.4. Bismuth-based photocatalysts

Bismuth-based photocatalyst materials such as bismuth oxide (Bi_2O_3), bismuth oxyhalides (such as BiOX, where X represents a halogen), and bismuth-based perovskites are a class of materials that have gained attention in recent years for their potential applications in various photocatalytic processes, including pollutant degradation, and solar energy conversion. Fortunately, there are reasonable studies involving the use of bismuth-based materials as photocatalysts to degrade OFL.

In the studies by Sood et al. [40], pristine Bi_2O_3 and a composite of Bi_2O_3/TiO_2 were used as photocatalysts to degrade OFL. Although the wavelength of Bi_2O_3 was 446 nm and that of the optimized Bi_2O_3/TiO_2 was 404.6 nm, the degradation efficiency of Bi_2O_3 towards OFL was 75% and that of optimized Bi_2O_3/TiO_2 was 92.4% in 120 min. Factors such as small size, high surface area etc. contributed to such performance.

The use of Bi_2WO_6, Bi_2WO_6/Fe_3O_4 and Bi_2WO_6/Fe_3O_4/BC as photocatalysts to degrade OFL have been reported by Wang et al. [41]. The introduction of biochar prevented the agglomeration of Bi_2WO_6 microspheres and Fe_3O_4 nanoparticles. On the other hand, Fe_3O_4 and biochar promoted charge separation and light absorption. Moreover, the Bi_2WO_6/Fe_3O_4/BC had the largest adsorption capacity. The degradation rate of Bi_2WO_6, Bi_2WO_6/Fe_3O_4 and Bi_2WO_6/Fe_3O_4/BC towards OFL were found to be 0.0347, 0.1295 and 0.1835 min^{-1}. Another ternary Bi_2MoO_6-rGO-TiO_2 photocatalyst have been used by Raja et al. [33] to degrade OFL. The degradation rate by Bi_2MoO_6, Bi_2MoO_6-rGO, Bi_2MoO_6-TiO_2 and Bi_2MoO_6-rGO-TiO_2 were found to be 0.0041, 0.0055, 0.0090 and 0.174 min^{-1}. The synergistic effect between Bi_2MoO_6-TiO_2 and rGO resulted in the higher performance by Bi_2MoO_6-rGO-TiO_2 compared to other catalysts.

Multiwalled carbon nanotubes (MWCNTs) have been used by Gao et al. [42] to form MWCNTs/Bi_5O_7I heterojunction to serve as photocatalyst to degrade OFL. Due to its ability to serve as photoelectrons transformation pathway, MWCNTs-[42]/[43] Bi_5O_7I degraded OFL at the rate of 0.0129 min^{-1}, compared to the rate by Bi_5O_7I which is just 0.0046 min^{-1}.

The role of cadmium doping in the performance of Bi_2MoO_6 towards photocatalytic degradation of OFL have been reported by Xu et al. [44]. Compared to pristine Bi_2MoO_6 with degradation rate 0.02978 min^{-1}, 1% Cd- Bi_2MoO_6 had the best degradation rate of 0.04839 min^{-1}. The introduction of Cd atom lowered the valence band (VB) and widened the bandgap of pristine Bi_2MoO_6, thereby enhancing its oxidation capacity and suppressing the recombination of charge carriers.

4.5. Others

Aside titanium-based, zinc-based, silver-based and bismuth-based photocatalysts, there are other catalysts that are being used/developed due to the interest in concept of degrading pollutants including OFL. Although degradation efficiency greater than 50% has been recorded using some catalysts including $La_2Ti_2O_7$ [45], CdS [46], NH_2-MIL-125 [47], g-C_3N_4 [48] etc. however, modification via doping, formation of heterojunction/composites have resulted in higher efficiencies.

For instance, Zhang et al. [49] reported the use of $Sm_2Ti_2O_7$ supported on quartz sand as photocatalyst to degrade OFL. An efficiency of 53.9% was achieved using pristine $Sm_2Ti_2O_7$, supporting the catalyst on quartz sand resulted in a higher efficiency of 99.2%. Although, the activity of photocatalysts usually reduced after loading on various supports, however, quartz sand is transparent to UV photons and, the lifetime of charge carriers is much longer in $Sm_2Ti_2O_7$ supported on quartz sand than in pristine $Sm_2Ti_2O_7$.

Yang et al. [50] reported the use of $Sm_2Ti_2O_7$, $Sm_2Ti_2O_7$/NaZSM-5 and $Sm_2Ti_2O_7$/HZSM-5 as photocatalysts to degrade OFL. HZSM-5 was prepared using NaZSM-5 via treatment with hydrochloric acid. On application, $Sm_2Ti_2O_7$, $Sm_2Ti_2O_7$/NaZSM-5 and $Sm_2Ti_2O_7$/HZSM-5 photocatalysts were able to degrade 45.1, 70 and 93.5% OFL in 150 min. The better performance recorded in the case $Sm_2Ti_2O_7$/HZSM-5 is attributed to the increased hydroxyl radicals production.

The effect of calcination temperature on the photocatalytic performance of porous cerium titanate has been studied by Wang et al. [51]. Initially, the fractions of $Ce_2Ti_2O_6$, CeO_2, anatase TiO_2 and rutile TiO_2 phases were found to vary with calcination temperature. The adsorption capacity of $Ce_2Ti_2O_6$ was found to drastically decrease with an increase in calcination temperature. However, the photocatalytic efficiency increased from 31.2 to 56.7% when the calcination temperature was raised from 600 to 800 ºC. Beyond 800 ºC, the material was found to lose its activity.

Interestingly, Shi et al. [52] reported the use of a composite of metal organic frameworks (UiO-66) and wood as a photocatalyst to degrade OFL under sunlight. The performance by UiO-66/wood was inspiring with a degradation rate constant 1.2 and 1.5 times higher than that of UiO-66 and wood. Such result was because, the presence of wood inhibited the recombination of charge carriers, thus improving the photocatalytic efficiency of UiO-66/wood.

5. Conclusion

From the above brief survey, photocatalytic degradation technology is a prominent method employed in the treatment of wastewater contaminated by ofloxacin, and efficient results have been reported using such approach. Notwithstanding, such efficient results are usually obtained after modification of the pristine photocatalysts via doping, formation of composites or construction of heterojunctions. In addition to such modifications, the morphology and surface area of the catalysts were found to have impact on their photocatalytic performance. However, most of the studies reported are results of laboratory scale experiments and not from real wastewater treatment plants. Similarly, studies on the photocatalytic degradation using immobilized composites should be explored for more convenient remediation process.

Acknowledgments

The authors received no financial support for the research, author-ship and/or publication of this article.

Conflict of interest

The authors declare that there is no conflict of interest.

REFERENCES

[1] D.H.K. Reddy, Water Pollution Control Technologies, (2017).
[2] C. Corada-Fernández, L. Candela, N. Torres-Fuentes, M.G. Pintado-Herrera, M. Paniw, E. González-Mazo, Effects of extreme rainfall events on the distribution of selected emerging contaminants in surface and groundwater: The Guadalete River basin (SW, Spain), Science of the total environment 605 (2017) 770-783.
[3] J. Li, K. Zhang, H. Zhang, Adsorption of antibiotics on microplastics, Environmental Pollution 237 (2018) 460-467.
[4] Y. Chen, T. Lan, L. Duan, F. Wang, B. Zhao, S. Zhang, W. Wei, Adsorptive removal and adsorption kinetics of fluoroquinolone by nano-hydroxyapatite, PLoS One 10(12) (2015) e0145025.
[5] K. He, A.D. Soares, H. Adejumo, M. McDiarmid, K. Squibb, L. Blaney, Detection of a wide variety of human and veterinary fluoroquinolone antibiotics in municipal wastewater and wastewater-impacted surface water, Journal of pharmaceutical and biomedical analysis 106 (2015) 136-143.
[6] R. Dong, G. Yu, Y. Guan, B. Wang, J. Huang, S. Deng, Y. Wang, Occurrence and discharge of pharmaceuticals and personal care products in dewatered sludge from WWTPs in Beijing and Shenzhen, Emerging Contaminants 2(1) (2016) 1-6.
[7] W. Wang, C. Zhai, Y. Peng, K. Chao, A Nondestructive Detection Method for Mixed Veterinary Drugs in Pork Using Line-Scan Raman Chemical Imaging Technology, Food Analytical Methods 12(3) (2019) 658-667.
[8] S. Sharma, A. Bhandari, V. Choudhary, H. Rajpurohit, P. Khandelwal, RP-HPLC method for simultaneous estimation of nitazoxanide and ofloxacin in tablets, Indian Journal of Pharmaceutical Sciences 73(1) (2011) 84.
[9] F. Janos, G.C. Robin, Analogue-based Drug Discovery, John Wiley and Sons, 2006.
[10] J. Sun, M. Song, J. Feng, Y. Pi, Highly efficient degradation of ofloxacin by UV/Oxone/Co^{2+} oxidation process, Environmental Science and Pollution Research 19(5) (2012) 1536-1543.
[11] K. Mushtaq, M. Saeed, W. Gul, M. Munir, A. Firdous, T. Yousaf, K. Khan, H.M.R. Sarwar, M.A. Riaz, S. Zahid, Synthesis and characterization of TiO_2 via sol-gel method for efficient photocatalytic degradation of antibiotic ofloxacin, Inorganic and Nano-Metal Chemistry (2020) 1-7.
[12] R. Kaur, J.P. Kushwaha, N. Singh, Electro-catalytic oxidation of ofloxacin antibiotic in continuous reactor: evaluation, transformation products and pathway, Journal of The Electrochemical Society 166(6) (2019) H250.
[13] T.-S. Chen, Y.-M. Kuo, J.-L. Chen, K.-L. Huang, Anodic degradation of ofloxacin on a boron-doped diamond electrode, Int. J. Electrochem. Sci 8 (2013) 7625-7633.
[14] M. Peres, M. Maniero, J. Guimarães, Photocatalytic degradation of ofloxacin and evaluation of the residual antimicrobial activity, Photochemical & Photobiological Sciences 14(3) (2015) 556-562.
[15] O.V. Enick, M.M. Moore, Assessing the assessments: pharmaceuticals in the environment, Environmental Impact Assessment Review 27(8) (2007) 707-729.
[16] B.R. Esposito, M.L. Capobianco, A. Martelli, M.L. Navacchia, L. Pretali, M. Saracino, A. Zanelli, S.S. Emmi, Advanced water remediation from ofloxacin by ionizing radiation, Radiation Physics and Chemistry 141 (2017) 118-124.
[17] N.S. Mishra, R. Reddy, A. Kuila, A. Rani, P. Mukherjee, A. Nawaz, S. Pichiah, A review on advanced oxidation processes for effective water treatment, Current World Environment 12(3) (2017) 470.
[18] S. Varnagiris, M. Urbonavicius, S. Sakalauskaite, R. Daugelavicius, L. Pranevicius, M. Lelis, D. Milcius, Floating TiO_2 photocatalyst for efficient inactivation of E. coli and decomposition of methylene blue solution, Science of The Total Environment 720 (2020) 137600.
[19] A.G. Leonel, A.A. Mansur, H.S. Mansur, Advanced functional nanostructures based on magnetic iron oxide nanomaterials for water remediation: a review, Water Research 190 (2021) 116693.
[20] S. Lu, C. Lin, K. Lei, B. Wang, M. Xin, X. Gu, Y. Cao, X. Liu, W. Ouyang, M. He, Occurrence, spatiotemporal variation, and ecological risk of antibiotics in the water of the semi-enclosed urbanized Jiaozhou Bay in eastern China, Water Research 184 (2020) 116187.
[21] R.A. Wuana, R. Sha'Ato, S. Iorhen, Aqueous phase removal of ofloxacin using adsorbents from Moringa oleifera pod husks, Advances in Environmental Research 4(1) (2015) 49-68.
[22] X. Wang, Y. Zhao, Y. Sun, D. Liu, Highly Effective Removal of Ofloxacin from Water with Copper-Doped ZIF-8, Molecules 27(13) (2022) 4312.
[23] Q. Su, J. Li, H. Yuan, B. Wang, Y. Wang, Y. Li, Y. Xing, Visible-light-driven photocatalytic degradation of ofloxacin by g-C_3N_4/NH_2-MIL-88B (Fe) heterostruc-

ture: Mechanisms, DFT calculation, degradation pathway and toxicity evolution, Chemical Engineering Journal 427 (2022) 131594.
[24] E. Gullberg, S. Cao, O.G. Berg, C. Ilbäck, L. Sandegren, D. Hughes, D.I. Andersson, Selection of resistant bacteria at very low antibiotic concentrations, PLoS pathogens 7(7) (2011) e1002158.
[25] J. Xue, S. Ma, Y. Zhou, Z. Zhang, M. He, Facile photochemical synthesis of Au/Pt/g-C_3N_4 with plasmon-enhanced photocatalytic activity for antibiotic degradation, ACS applied materials & interfaces 7(18) (2015) 9630-9637.
[26] X.-q. Cao, F. Xiao, Z.-w. Lyu, X.-y. Xie, Z.-x. Zhang, X. Dong, J.-x. Wang, X.-j. Lyu, Y.-z. Zhang, Y. Liang, $CuFe_2O_4$ supported on montmorillonite to activate peroxymonosulfate for efficient ofloxacin degradation, Journal of Water Process Engineering 44 (2021) 102359.
[27] H. Abdullah, M.M.R. Khan, H.R. Ong, Z. Yaakob, Modified TiO_2 photocatalyst for CO_2 photocatalytic reduction: an overview, Journal of CO2 Utilization 22 (2017) 15-32.
[28] X. Wang, Z. Hu, Y. Chen, G. Zhao, Y. Liu, Z. Wen, A novel approach towards high-performance composite photocatalyst of TiO_2 deposited on activated carbon, Applied Surface Science 255(7) (2009) 3953-3958.
[29] S. Chen, Y. Liu, Study on the photocatalytic degradation of glyphosate by TiO_2 photocatalyst, Chemosphere 67(5) (2007) 1010-1017.
[30] O. Ola, M.M. Maroto-Valer, Review of material design and reactor engineering on TiO_2 photocatalysis for CO_2 reduction, Journal of Photochemistry and Photobiology C: Photochemistry Reviews 24 (2015) 16-42.
[31] R. Kaur, A. Kaur, R. Kaur, S. Singh, M.S. Bhatti, A. Umar, S. Baskoutas, S.K. Kansal, Cu-BTC metal organic framework (MOF) derived Cu-doped TiO_2 nanoparticles and their use as visible light active photocatalyst for the decomposition of ofloxacin (OFX) antibiotic and antibacterial activity, Advanced Powder Technology 32(5) (2021) 1350-1361.
[32] V. Bhatia, A.K. Ray, A. Dhir, Enhanced photocatalytic degradation of ofloxacin by co-doped titanium dioxide under solar irradiation, Separation and Purification Technology 161 (2016) 1-7.
[33] A. Raja, N. Son, M. Kang, Construction of visible-light driven Bi_2MoO_6-rGO-TiO_2 photocatalyst for effective ofloxacin degradation, Environmental Research 199 (2021) 111261.
[34] A. Kaur, A. Umar, W.A. Anderson, S.K. Kansal, Facile synthesis of CdS/TiO_2 nanocomposite and their catalytic activity for ofloxacin degradation under visible illumination, Journal of Photochemistry and Photobiology A: Chemistry 360 (2018) 34-43.
[35] K. Karthik, A. Raghu, K.R. Reddy, R. Ravishankar, M. Sangeeta, N.P. Shetti, C.V. Reddy, Green synthesis of Cu-doped ZnO nanoparticles and its application for the photocatalytic degradation of hazardous organic pollutants, Chemosphere 287 (2022) 132081.
[36] A.M. Saad, M.R. Abukhadra, S.A.-K. Ahmed, A.M. Elzanaty, A.H. Mady, M.A. Betiha, J.-J. Shim, A.M. Rabie, Photocatalytic degradation of malachite green dye using chitosan supported ZnO and Ce–ZnO nano-flowers under visible light, Journal of environmental management 258 (2020) 110043.
[37] A. Kaur, G. Gupta, A.O. Ibhadon, D.B. Salunke, A. Sinha, S.K. Kansal, A Facile synthesis of silver modified ZnO nanoplates for efficient removal of ofloxacin drug in aqueous phase under solar irradiation, Journal of Environmental Chemical Engineering 6(3) (2018) 3621-3630.
[38] T. Chankhanittha, N. Komchoo, T. Senasu, J. Piriyanon, S. Youngme, K. Hemavibool, S. Nanan, Silver decorated ZnO photocatalyst for effective removal of reactive red azo dye and ofloxacin antibiotic under solar light irradiation, Colloids and Surfaces A: Physicochemical and Engineering Aspects 626 (2021) 127034.
[39] J. Piriyanon, P. Takhai, S. Patta, T. Chankhanittha, T. Senasu, S. Nijpanich, S. Juabrum, N. Chanlek, S. Nanan, Performance of sunlight responsive WO_3/AgBr heterojunction photocatalyst toward degradation of Rhodamine B dye and ofloxacin antibiotic, Optical Materials 121 (2021) 111573.
[40] S. Sood, S.K. Mehta, A. Sinha, S.K. Kansal, Bi_2O_3/TiO_2 heterostructures: synthesis, characterization and their application in solar light mediated photocatalyzed degradation of an antibiotic, ofloxacin, Chemical Engineering Journal 290 (2016) 45-52.
[41] Z. Wang, X. Cai, X. Xie, S. Li, X. Zhang, Z. Wang, Visible-LED-light-driven photocatalytic degradation of ofloxacin and ciprofloxacin by magnetic biochar modified flower-like Bi_2WO_6: The synergistic effects, mechanism insights and degradation pathways, Science of The Total Environment 764 (2021) 142879.
[42] P. Gao, S. Huang, K. Tao, Z. Li, L. Feng, Y. Liu, L. Zhang, Synthesis of adjustable {312}/{004} facet heterojunction MWCNTs/Bi_5O_7I photocatalyst for ofloxacin degradation: Novel insights into the charge carriers transport, Journal of Hazardous Materials 437 (2022) 129374.
[43] G. Gupta, S.K. Kansal, A. Umar, S. Akbar, Visible-light driven excellent photocatalytic degradation of ofloxacin antibiotic using $BiFeO_3$ nanoparticles, Chemosphere 314 (2023) 137611.
[44] J. Xu, Y. Liu, M. Chen, Preparation of Cd-doped Bi_2MoO_6 photocatalyst for efficient degradation of ofloxacin under the irradiation of visible light, Surfaces and Interfaces 25 (2021) 101246.
[45] H. Wang, Y. Zhang, Z. Ma, W. Zhang, Role of PEG2000 on sol-gel preparation of porous $La_2Ti_2O_7$ for enhanced photocatalytic activity on ofloxacin degradation, Materials Science in Semiconductor Processing 91 (2019) 151-158.
[46] T. Senasu, N. Ruengchai, S. Khamdon, N. Lorwanishpaisarn, S. Nanan, Hydrothermal Synthesis of Cadmium Sulfide Photocatalyst for Detoxification of Azo Dyes and Ofloxacin Antibiotic in Wastewater, Molecules 27(22) (2022) 7944.
[47] H. Alamgholiloo, N.N. Pesyan, A.P. Marjani, Visible-light-responsive Z-scheme α-Fe_2O_3/SWCNT/NH_2-MIL-125 heterojunction for boosted photodegradation of ofloxacin, Separation and Purification Technology 305 (2023) 122442.
[48] L. Hou, W. Li, Z. Wu, Q. Wei, H. Yang, Y. Jiang, T. Wang, Y. Wang, Q. He, Embedding ZnCdS@ $ZnIn_2S_4$ into thiazole-modified g-C_3N_4 by electrostatic self-assembly to build dual Z-scheme heterojunction with spatially separated active centers for photocatalytic H_2 evolution and ofloxacin degradation, Separation and Purification Technology 290 (2022) 120858.
[49] T. Zhang, W. Zhang, H. Li, L. Yang, W. Xu, Enhanced photocatalytic degradation of ofloxacin by $Sm_2Ti_2O_7$ supported on quartz sand, Materials Science in Semiconductor Processing 158 (2023) 107354.
[50] L. Yang, K. Wang, J. Yang, W. Zhang, Role of hydrochloric acid treated HZSM-5 zeolite in $Sm_2Ti_2O_7$/nHZSM-5 composite for photocatalytic degradation of ofloxacin, Journal of Materials Research and Technology 9(5) (2020) 10585-10596.
[51] H. Wang, M. Han, Y. Zhou, J. Li, X. Xiao, W. Zhang, Effects of thermal treatment on porous cerium titanate photocatalyst for ofloxacin degradation, Journal of Nanoscience and Nanotechnology 19(8) (2019) 5264-5270.
[52] L. Shi, X. Zou, T. Wang, D. Wang, M. Fan, Z. Gong, Sunlight photocatalytic degradation of ofloxacin using UiO-66/wood composite photocatalysts, Chinese Chemical Letters 33(1) (2022) 442-446.
[53] L. Wang, N. Liang, H. Li, Y. Yang, D. Zhang, S. Liao, B. Pan, Quantifying the dynamic fluorescence quenching of phenanthrene and ofloxacin by dissolved humic acids, Environmental pollution 196 (2015) 379-385.
[54] C. Wang, D. Dong, L. Zhang, Z. Song, X. Hua, Z. Guo, Response of freshwater biofilms to antibiotic florfenicol and ofloxacin stress: role of extracellular polymeric substances, International journal of environmental research and public health 16(5) (2019) 715.
[55] I. Michael, E. Hapeshi, C. Michael, D. Fatta-Kassinos, Solar Fenton and solar TiO_2 catalytic treatment of ofloxacin in secondary treated effluents: evaluation of operational and kinetic parameters, Water research 44(18) (2010) 5450-5462.
[56] C. El Bekkali, H. Bouyarmane, S. Laasri, M. El Karbane, A. Saoiabi, A. Laghzizil, Sorption and photocatalytic degradation of ciprofloxacin and ofloxacin in aqueous suspensions of TiO_2 and ZnO catalysts, (2017).
[57] Q. Kong, X. He, L. Shu, M.-s. Miao, Ofloxacin adsorption by activated carbon derived from luffa sponge: Kinetic, isotherm, and thermodynamic analyses, Process Safety and Environmental Protection 112 (2017) 254-264.
[58] U. Onyenze, O.I. Edozie, Synthesis, Spectroscopic Characterization and Antibactrial Activities of Co (II) Complex of Ofloxacin Drug Mixed with Ascorbic Acid as a Secondary Ligand, BioScientific Review 3(3) (2021) 1-12.
[59] E. Hapeshi, A. Achilleos, A. Papaioannou, L. Valanidou, N.P. Xekoukoulotakis, D. Mantzavinos, D. Fatta-Kassinos, Sonochemical degradation of ofloxacin in aqueous solutions, Water Science and Technology 61(12) (2010) 3141-3146.
[60] D.N.R. de Sousa, S. Insa, A.A. Mozeto, M. Petrovic, T.F. Chaves, P.S. Fadini, Equilibrium and kinetic studies of the adsorption of antibiotics from aqueous solutions onto powdered zeolites, Chemosphere 205 (2018) 137-146.
[61] C. Ding, J. Guo, P. Chen, W. Gan, Z. Yin, S. Qi, M. Zhang, Z. Sun, All-solid-state Z-scheme In_2S_3/CQDs/TiO_2 heterojunction for highly efficient degradation of ofloxacin, Applied Surface Science 596 (2022) 153629.
[62] C. Ye, W. Zhang, Y. Liu, Supporting B–TiO_2 on iM16K glass bubbles to prepare B–TiO_2 (x%)/iM16K hollow spheres for ofloxacin degradation, Ceramics International 46(8) (2020) 10545-10554.
[63] S. Zhang, Y. Wang, Z. Cao, J. Xu, J. Hu, Y. Huang, C. Cui, H. Liu, H. Wang, Simultaneous enhancements of light-harvesting and charge transfer in UiO-67/CdS/rGO composites toward ofloxacin photo-degradation, Chemical Engineering Journal 381 (2020) 122771.
[64] M.S. Kanza Mushtaq, W. Gul, M. Munir, A. Firdous, T. Yousaf, K. Khan, H.M. Rizwan, M.A.R. Sarwar, S. Zahid, Synthesis and characterization of TiO_2 via sol-gel method for efficient photocatalytic degradation of antibiotic ofloxacin, .
[65] T. Chankhanittha, S. Nanan, Visible-light-driven photocatalytic degradation of ofloxacin (OFL) antibiotic and Rhodamine B (RhB) dye by solvothermally grown ZnO/Bi_2MoO_6 heterojunction, Journal of Colloid and Interface Science 582

(2021) 412-427.
[66] A.İ. Vaizoğullar, Ternary CdS/MoS2/ZnO photocatalyst: synthesis, characterization and degradation of ofloxacin under visible light irradiation, Journal of Inorganic and Organometallic Polymers and Materials 30(10) (2020) 4129-4141.
[67] W. Ning, Z. Zhao, H. Chang, Z. Gu, B. Zhang, S. Yin, J. Fan, Photocatalytic degradation of ofloxacin by ZnO/Cs_xWO_3 composite synthesized by two-step method: A kinetic study, Functional Materials Letters 12(05) (2019) 1950068.
[68] T. Senasu, T. Chankhanittha, K. Hemavibool, S. Nanan, Visible-light-responsive photocatalyst based on ZnO/CdS nanocomposite for photodegradation of reactive red azo dye and ofloxacin antibiotic, Materials Science in Semiconductor Processing 123 (2021) 105558.
[69] J. Jia, Y. Liang, G. Yang, J. Yang, X. Zhang, Z. Zeng, Z. Yang, S. Xu, C. Han, Reinforced $AgFeO_2$-Bi_4TaO_8Cl pn heterojunction with facet-assisted photocarrier separation for boosting photocatalytic degradation of ofloxacin, Separation and Purification Technology (2023) 124333.
[70] R. Chen, S. Ding, N. Fu, X. Ren, Preparation of a g-C_3N_4/Ag_3PO_4 composite Z-type photocatalyst and photocatalytic degradation of Ofloxacin: Degradation performance, reaction mechanism, degradation pathway and toxicity evaluation, Journal of Environmental Chemical Engineering 11(2) (2023) 109440.
[71] H. Yin, H. Shi, L. Sun, D. Xia, X. Yuan, Construction of Ag_2O-modified gC_3N_4 photocatalyst for rapid visible light degradation of ofloxacin, Environmental Science and Pollution Research 28 (2021) 11650-11664.
[72] G. Gupta, A. Umar, A. Kaur, S. Sood, A. Dhir, S. Kansal, Solar light driven photocatalytic degradation of Ofloxacin based on ultra-thin bismuth molybdenum oxide nanosheets, Materials Research Bulletin 99 (2018) 359-366.
[73] S. Adhikari, D.-H. Kim, Synthesis of Bi_2S_3/Bi_2WO_6 hierarchical microstructures for enhanced visible light driven photocatalytic degradation and photoelectrochemical sensing of ofloxacin, Chemical Engineering Journal 354 (2018) 692-705.
[74] M. Zhang, J. Xu, M. Chen, Novel Z-scheme $LaVO_4$/Bi_3O_4Cl heterojunctions for highly efficient degradation of ofloxacin under visible light irradiation, Journal of Alloys and Compounds 925 (2022) 166653.
[75] J. Xu, B. Feng, Y. Wang, Y. Qi, J. Niu, M. Chen, BiOCl decorated $NaNbO_3$ nanocubes: a novel pn heterojunction photocatalyst with improved activity for ofloxacin degradation, Frontiers in Chemistry 6 (2018) 393.
[76] S. Mandal, S. Adhikari, S. Choi, Y. Lee, D.-H. Kim, Fabrication of a novel Z-scheme Bi_2MoO_6/GQDs/MoS_2 hierarchical nanocomposite for the photo-oxidation of ofloxacin and photoreduction of Cr (VI) as aqueous pollutants, Chemical Engineering Journal 444 (2022) 136609.
[77] J. Jia, Y. Liang, G. Yang, J. Yang, X. Zhang, Z. Xiong, K. Sa, Z. Zeng, Y. Han, Molten-salt-mediated synthesis of Na^+ doped Bi_4TaO_8Cl nanosheets with exposed {001} facets for enhanced photocatalytic degradation, Journal of Alloys and Compounds 932 (2023) 167461.
[78] P. Dhiman, G. Sharma, A.N. Alodhayb, A. Kumar, G. Rana, T. Sithole, Z.A. ALOthman, Constructing a Visible-Active $CoFe_2O_4$@ Bi_2O_3/NiO Nanoheterojunction as Magnetically Recoverable Photocatalyst with Boosted Ofloxacin Degradation Efficiency, Molecules 27(23) (2022) 8234.
[79] W. Zhang, J. Yang, C. Li, Role of thermal treatment on sol-gel preparation of porous cerium titanate: characterization and photocatalytic degradation of ofloxacin, Materials Science in Semiconductor Processing 85 (2018) 33-39.
[80] W. Zhang, Y. Liu, C. Li, Photocatalytic degradation of ofloxacin on $Gd_2Ti_2O_7$ supported on quartz spheres, Journal of Physics and Chemistry of Solids 118 (2018) 144-149.
[81] D. Zhang, J. Qi, H. Ji, S. Li, L. Chen, T. Huang, C. Xu, X. Chen, W. Liu, Photocatalytic degradation of ofloxacin by perovskite-type $NaNbO_3$ nanorods modified g-C_3N_4 heterojunction under simulated solar light: Theoretical calculation, ofloxacin degradation pathways and toxicity evolution, Chemical Engineering Journal 400 (2020) 125918.
[82] M. Kaur, S.K. Mehta, S.K. Kansal, Visible light driven photocatalytic degradation of ofloxacin and malachite green dye using cadmium sulphide nanoparticles, Journal of environmental chemical engineering 6(3) (2018) 3631-3639.
[83] G. Sharma, A. Kumar, P.S. Kumar, A. Alodhayb, Z.A. ALOthman, P. Dhiman, F.J. Stadler, Carbon quantum dots embedded trimetallic oxide: Characterization and photocatalytic degradation of Ofloxacin, Journal of Water Process Engineering 48 (2022) 102853.
[84] K. Saravanakumar, G. Mamba, V. Muthuraj, 1D/2D $MnWO_4$ nanorods anchored on g-C_3N_4 nanosheets for enhanced photocatalytic degradation ofloxacin under visible light irradiation, Colloids and Surfaces A: Physicochemical and Engineering Aspects 581 (2019) 123845.
[85] S.-W. Lv, J.-M. Liu, N. Zhao, C.-Y. Li, Z.-H. Wang, S. Wang, Benzothiadiazole functionalized Co-doped MIL-53-NH2 with electron deficient units for enhanced photocatalytic degradation of bisphenol A and ofloxacin under visible light, Journal of hazardous materials 387 (2020) 122011.
[86] S. Sharma, S. Basu, Visible-light-induced photocatalytic response of easily recoverable Mn_2O_3/SiO_2 monolith in centimeter-scale towards degradation of ofloxacin: Performance evaluation and product analysis, Chemosphere 307 (2022) 135973.
[87] X. Feng, X. Li, B. Su, Photocatalytic degradation performance of antibiotics by peanut shell biochar anchored NiCr-LDH nanocomposites fabricated by one-pot hydrothermal protocol, Colloids and Surfaces A: Physicochemical and Engineering Aspects 666 (2023) 131337.
[88] D. Liu, J. Gong, C. Sun, L. Xu, Y. Song, Enhanced photocatalytic activity for degradation of ofloxacin and dye by hierarchical flower-like ZnS/MoS_2/Bi_2WO_6 heterojunction: Synergetic effect of 2D/2D coupling interface and solid sulfide solutions, Catalysis Communications 172 (2022) 106546.
[89] W. Zhang, Y. Tao, C. Li, Sol-gel synthesis of $Gd_2Ti_2O_7$/HZSM-5 composite photocatalyst for ofloxacin degradation, Journal of Photochemistry and Photobiology A: Chemistry 364 (2018) 787-793.
[90] S. Adhikari, H.H. Lee, D.-H. Kim, Efficient visible-light induced electron-transfer in z-scheme MoO_3/Ag/C_3N_4 for excellent photocatalytic removal of antibiotics of both ofloxacin and tetracycline, Chemical Engineering Journal 391 (2020) 123504.
[91] Q. Wei, H. Yang, W. Li, T. Wang, L. Hou, Z. Wu, Y. Jiang, Efficient photocatalytic H_2 production and ofloxacin degradation based on heterodimensional Z-scheme P-C_3N_4/MIL-88A (Fe) heterojunctions, Journal of Alloys and Compounds 920 (2022) 165980.
[92] H. Jia, D. Ma, S. Zhong, L. Li, L. Li, L. Xu, B. Li, Boosting photocatalytic activity under visible-light by creation of PCN-222/g-C_3N_4 heterojunctions, Chemical Engineering Journal 368 (2019) 165-174.